Biomaterials 95 (2016) 47–59

Contents lists available at ScienceDirect

Biomaterials

journal homepage: www.elsevier.com/locate/biomaterials

Metabolic response of lung cancer cells to radiation in a paper-based 3D cell culture system

Karen A. Simon [a], Bobak Mosadegh [a, b, c], Kyaw Thu Minn [a], Matthew R. Lockett [a, d], Marym R. Mohammady [a], Diane M. Boucher [e], Amy B. Hall [e], Shawn M. Hillier [e], Taturo Udagawa [e], Brenda K. Eustace [e, **], George M. Whitesides [a, b, *]

[a] Department of Chemistry and Chemical Biology, Harvard University, 12 Oxford Street, Cambridge, MA 02138, USA
[b] Wyss Institute for Biologically Inspired Engineering, Harvard University, 60 Oxford Street, Cambridge, MA 02138, USA
[c] Dalio Institute of Cardiovascular Imaging, Department of Radiology, Weill Cornell Medicine, 413 E. 69th Street Suite BRB-108, New York, NY 10021, USA
[d] Department of Chemistry, University of North Carolina at Chapel Hill, 125 South Road, Chapel Hill, NC 27599, USA
[e] Vertex Pharmaceuticals Incorporated, 50 Northern Blvd., Boston, MA 02210, USA

ARTICLE INFO

Article history:
Received 4 September 2015
Received in revised form
29 February 2016
Accepted 2 March 2016
Available online 3 March 2016

Keywords:
Tumor hypoxia
Radiation response
3D cell culture
Oxygen gradients
Radioresistance

ABSTRACT

This work demonstrates the application of a 3D culture system—**C**ells-**i**n-**G**els-**i**n-**P**aper (CiGiP)—in evaluating the metabolic response of lung cancer cells to ionizing radiation. The 3D tissue-like construct—prepared by stacking multiple sheets of paper containing cell-embedded hydrogels—generates a gradient of oxygen and nutrients that decreases monotonically in the stack. Separating the layers of the stack after exposure enabled analysis of the cellular response to radiation as a function of oxygen and nutrient availability; this availability is dictated by the distance between the cells and the source of oxygenated medium. As the distance between the cells and source of oxygenated media increased, cells show increased levels of hypoxia-inducible factor 1-alpha, decreased proliferation, and reduced sensitivity to ionizing radiation. Each of these cellular responses are characteristic of cancer cells observed in solid tumors. With this setup we were able to differentiate three isogenic variants of A549 cells based on their metabolic radiosensitivity; these three variants have known differences in their metastatic behavior *in vivo*. This system can, therefore, capture some aspects of radiosensitivity of populations of cancer cells related to mass-transport phenomenon, carry out systematic studies of radiation response *in vitro* that decouple effects from migration and proliferation of cells, and regulate the exposure of oxygen to subpopulations of cells in a tissue-like construct either before or after irradiation.

1. Introduction

In the United States and many developed countries, the overall 5-year survival rate of a patient with lung cancer is estimated to be between 15 and 20% [1,2]. One-third of lung cancer patients are diagnosed at an advanced stage, and radiation therapy remains a preferred strategy for targeting these tumorigenic cells, which possess compromised DNA repair machinery and often proliferate at higher rates than normal cells [3–5]. Cells exposed to ionizing radiation ultimately die from damage to DNA: directly in the form of induced single- or double-strand breaks, or indirectly by newly generated free radicals reacting with the DNA [6–15]. Cells can respond to ionizing radiation in multiple ways: (i) repairing the damage directly; (ii) undergoing cell cycle-arrest, which can lead to irreversible arrest (called senescence); or (iii) inducing programmed cell death (apoptosis), and (iv) cell death following the proliferation of damaged cells, or so-called "mitotic catastrophe" [9,16–20].

Oxygen plays a significant role in radiation therapy and is believed to act as a radio-sensitizer, leading to the production of free radical species that ultimately damage DNA [21]. To support the metabolic needs of cells, they should be no more than 150–200 μm away from a capillary to receive adequate concentrations of oxygen and other molecules (e.g., glucose, autocrine

* Corresponding author. Department of Chemistry and Chemical Biology, Harvard University, 12 Oxford Street, Cambridge, MA 02138, USA.
** Corresponding author.
E-mail addresses: brenda_eustace@vrtx.com (B.K. Eustace), gwhitesides@gmwgroup.harvard.edu (G.M. Whitesides).

http://dx.doi.org/10.1016/j.biomaterials.2016.03.002
0142-9612/

factors) [22–25]. Solid tumors are poorly vascularized and result in subpopulations of cells experiencing levels of decreased oxygen tension. Cells experiencing oxygen tensions of less than 10 mmHg are hypoxic; a phenotype that is often associated with poor clinical outcomes, tumor recurrence, and diminished sensitivity to chemotherapy and radiotherapy [26–33]. Elucidating the mechanisms by which cancer cells survive radiation therapy is a key to discovering novel therapies to improve patient outcome and prevent tumor recurrence.

Current *in vitro* models in radiobiology evaluate cellular response based on changes in either metabolism or proliferation following exposure to radiation. These models utilize cells grown as a monolayer on a solid surface or in a 3D format such as a spheroid or cells embedded in hydrogel slabs. While 2D cultures are easy to setup and maintain, they fail to mimic many aspects of a tissue because the cells lack the 3D contacts formed between adjacent cells and with extracellular matrix, and the 3D structural features of tissue that limit the mass transport of molecules within the culture environment [34,35]. These factors are crucial to the response of cells to chemo- and radio-therapy [36]. Spheroids provide a more realistic 3D microenvironment for cells than monolayer cultures, and due to their diffusion-limited environment are often used as models to study the localization of oxygen, other nutrients, or drugs in solid tumors [37–40]. The analysis of spheroids can be challenging because: (i) dissociation of the intact spheroid into a suspension of single cells prevents spatial analysis of the heterogeneity in the spheroid, (ii) histology requires fixation of cells, thus preventing further culture of these cells, and (iii) the heterogeneity in the size of the spheroids can affect the reproducibility of responses to drug or radiation assays.

We adapted the **C**ells-**i**n **G**els-**i**n-**P**aper, or CiGiP [41–43], system to evaluate the response of cells to increasing doses of ionizing radiation in 3D cultures. In this work, we prepared a scaffold composed of paper-plastic composite (Fig. 1A) to support the cell-laden gels; previous versions of this system utilized sheets of wax-patterned paper or mesh [42,44–47]. We chose these composite scaffolds (Fig. 1A) because they require fewer steps to fabricate than the paraffin film-patterned mesh sheet, and utilize a hydrophobic barrier that prevents the lateral diffusion of oxygen more efficiently than wax-printed sheets of paper [42,47]. These composites, which were patterned to contain hydrophilic openings that support the culture of cell-laden gels, were stacked to form thick tissue-like constructs. These multi-layer cultures were placed in an acrylic holder (Fig. 1B) that allowed us to control the exchange of fresh medium with the stack, and generate monotonically decreasing gradients—from top to bottom of the stack—of nutrients. Overlapping gradients of factors and cellular byproducts (e.g., carbon dioxide, lactate, cytokines) secreted by the cells were also formed in these setups. This culture format mimics two features of a poorly vascularized solid tumor, because: (i) Cells at the top of the stack readily exchange with fresh medium; these cells experience a well-oxygenated (normoxic) environment similar to cells in a tumor that are near a blood vessel. (ii) Cells at the bottom of the stack do not have access to fresh medium and experience an oxygen-poor (hypoxic) environment similar to cells in a region of a tumor that is far from a blood vessel.

2. Materials and methods

2.1. Materials and reagents

Polyvinyl chloride (PVC) sheets with a thickness of ~130 μm were obtained from Warp Bros. (Chicago, IL). Whatman 105 lens paper with a thickness of ~40 μm was purchased from GE Healthcare Biosciences (Pittsburgh, PA). Sheets of poly(methyl methacrylate) (PMMA) were purchased from McMaster-Carr (Princeton, NJ) and machined to prepare the custom-built holders used in this work. We purchased the A549 cells from American Type and Culture Collection (Manasas, VA). Supplies for cell culture and cell labeling such as Dulbecco's Modified Eagle Medium (DMEM), penicillin-streptomycin, TrypLE™ Express, and Click-iT® EdU were purchased from Life Technologies (Grand Island, NY). Fetal bovine serum (FBS) was purchased from HyClone (Logan, Utah), growth factor-reduced Matrigel was purchased from Corning (Tewksbury, MA), and RIPA buffer was purchased from Teknova (Hollister, CA). For immunoblotting, primary antibodies were purchased from Cell Signaling Technologies (Danvers, MA) and R&D Systems (Minneapolis, MN); secondary antibodies and Odyssey® blocking buffer were purchased from LI-COR Biosciences (Lincoln, Nebraska).

2.2. Preparing the composite sheets

We used a Graphtec Craft ROBO Pro Craft Cutter (Irvine, CA) to prepare the sheets of perforated polyvinyl chloride (PVC) shown in Fig. 1A; the pattern contains ten (~3 mm in diameter) perforations and was designed in Adobe Illustrator C4. We sandwiched the patterned sheet of polyvinyl chloride (PVC) between two sheets of Whatman 105 lens paper, and heat pressed the sheets together (215 °C, three to four cycles of 10–15 s) to form a single composite whose thickness is ~130 μm. A photograph of the assembled composite is provided in Fig. S-1. We refer to each of the perforations in the composite as a single "zone". Prior to usage, the composites were autoclaved in a glass petri dish, air-dried in a laminar flow hood, and then exposed to UV light for 1 h.

2.3. Seeding of cells into the composite sheets

We maintained all cell lines in vented tissue culture flasks in a 5% CO_2 at 37 °C environment; each flask contained DMEM with 5% FBS and 1% penicillin-streptomycin. Prior to seeding the composite sheets, we prepared a suspension of cells with cold Matrigel (4 °C). All experiments used a cell density of 2000 cells/μL, unless stated otherwise. To prepare the suspension of cells, we detached the cells from the flasks with TrypLE™ Express (5 min at 37 °C), washed them in medium, and then pelleted them by centrifugation at 1500 rpm. We spotted 1 μL of the suspension into each zone of the composite with a micropipette and then incubated the composite in a 6-well plate containing warm (37 °C) culture medium for at least 12 h prior to stacking or exposure to ionizing radiation. The cold suspension wicks into the composite and fills the zone; the Matrigel forms a gel upon warming (37 °C).

2.4. Preparing single-layer and multi-layer cultures

We refer to a single, cell-containing composite that is maintained in culture medium as a "single layer culture" (Fig. 1A). We refer to a stack of composite sheets, each containing cell-embedded gels, maintained in culture medium as a "multi-layer culture" (Fig 1B). Each of the multi-layer cultures discussed in this work consisted of six layers. For convenience, we refer to these layers as L1 through L6, where L1 is the topmost layer of the stack. The multi-layer cultures were placed in a custom-made acrylic holder (Fig. S-1) comprising a solid bottom base and a perforated top piece with holes whose position correspond to the zones of the composite. Both pieces of the holders were also equipped with threaded holes to fit screws, which ensured the sheets are held in conformal contact after stacking. Assembled multi-layer cultures were incubated in petri dishes containing warm (37 °C) culture medium. Prior to usage, the holders were autoclaved in a glass petri dish and

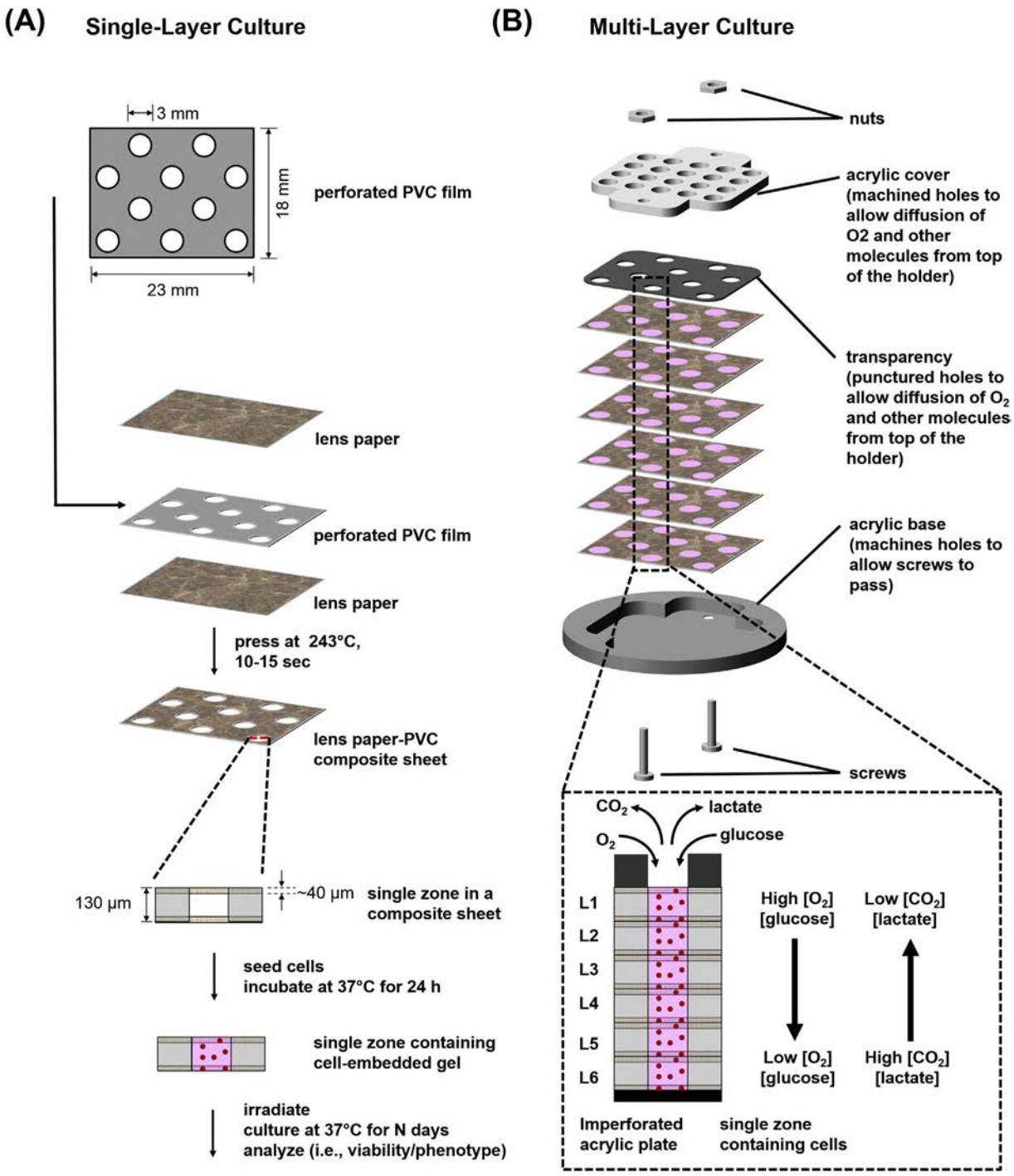

Fig. 1. Cell-in-Gels-in-Paper Cultures for Radiotherapy Assays. (A) Schematic of the fabrication of the composites sheets used for single-layer culture. (B) Schematic of the multi-layer culture, whose collective thickness is 0.78 mm (6 layers × 130 µm thick/layer = 0.78 mm thick). Unless otherwise stated, cells were seeded at a density of 2000 cells/zone, cultured as single layers overnight, stacked, cultured as a stack for four days, irradiated at 8 Gy, and cultured for seven days before analysis.

dried in a laminar flow hood.

Unless stated otherwise, we incubated the multi-layer cultures for at least four days prior to irradiation; this time period ensured a gradient in oxygen and nutrients formed in the stack.

2.5. Irradiation experiments

The samples were exposed to ionizing radiation from a GammaCell 40 Extractor Cesium-137 irradiator, which emits 1 Gy min^{-1} (Best Theratonics, Ontario, Canada). The samples were incubated for 6–7 days post-irradiation before metabolic activity, senescence, and rates of proliferation were measured.

2.6. Measurement of metabolic activity by CellTiter-Glo® (CTG) assay

We measured the metabolic activity of the cells using the CellTiter-Glo® (CTG) assay, which quantifies the total concentration of

ATP in a solution of lysed cells [48]. Multi-layer cultures were de-stacked by disassembling the holder and separating the individual sheets with tweezers. Each sheet was washed in 1X PBS (5 min, room temperature) and lysed in 1 mL RIPA buffer on an orbital shaker (10 min, 4 °C, ~160 rpm). The lysates were diluted in 1X PBS (1:10 by volume) and 100 μL was transferred into the wells of a black 96-well plate with a clear bottom. We prepared the CTG reagent by following the manufacturer's protocol, added 100 μL of CTG reagent to each lysate-containing well, incubated the plate for 20 min, and measured the luminescence of the samples using a Perkin Elmer Wallac Luminometer (Waltham, MA) or a BMG Labtech PHERAstar FS microplate reader (Ortenberg, Germany). For each scaffold, we took eight measurements (i.e., n = 8 wells) for CTG assay, calculated the average luminescence, and used this average value in calculating the number of metabolically-active cells based on a calibration curve; multiple stacks were conducted to produce errors bars for each layer.

2.7. Evaluation of senescence-associated β-galactosidase activity

We recovered A549-GFP cells from the composite sheets by incubating the samples in warm (37 °C) Accumax, which selectively degrades the Matrigel, for 30–45 min. The cells were pelleted by centrifugation (~1500 rpm), resuspended in culture medium (10,000 A549-GFP cells/mL), dispensed into a 96-well plate (100 μL/well), and cultured them overnight. We stained the cells with Millipore Cellular Senescence Assay Kit (Cat. KA002) according to the manufacturer's suggested protocol. We collected images of each well with a bright field microscope and enumerated the senescent cells, which were blue in color. We also collected images of the cells using a fluorescence microscope and counted the total number of GFP-expressing cells.

2.8. Proliferation assay

We used a Click-iT® EdU kit to label A549-GFP cells undergoing proliferation. In brief, we incubated each composite sheet in culture medium containing 10 μM EdU (24 h at 37 °C and 5% CO_2). The EdU-labeled samples were then fixed with 4% paraformaldehyde for 20 min, washed with 3% (v/v) BSA in 1X PBS (5 min × 3), incubated in 0.5% (v/v) Triton X-100 (20 min), washed with 3% (v/v) BSA in 1X PBS (5 min × 3), and incubated in Click-iT® reaction cocktail for 30 min. The Click-iT® reaction cocktail, which contained either an Alexa Fluor® 594-conjugated azide or an Alexa Fluor® 488-conjugated azide and 4 mM copper (II) sulfate was prepared based on manufacturer's suggested protocol. The samples were washed once with 3% BSA in 1X PBS (5 min) and kept in 1X PBS (4 °C). The composite sheets were imaged with a Typhoon Gel Scanner: Alexa Fluor® 594 was imaged with a 532 nm (excitation)/615 nm (emission) filter, PMT value of 400 V, and resolution of 50 μm; GFP was imaged with a 473 nm (excitation)/519 nm (emission) filter, PMT value of 300 V, and resolution of 50 μm.

2.9. Western blot analysis

Multi-layer cultures were de-stacked by disassembling the holder and separating the sheets with tweezers. Each sheet was washed in 1X PBS (5 min, room temperature) and then lysed in 500 μL RIPA buffer on an orbital shaker (30 min, 4 °C, ~160 rpm). We quantified the total protein content for each lysate using a BCA (bicichoninic acid) Assay, following the manufacturer's protocol. We prepared the protein-containing samples (0.5 μg/μL protein) in 1X NuPAGE® sample reducing buffer and 1X NuPAGE® LDS sample buffer. The protein-containing solutions were heated at 100 °C for 10 min, centrifuged at 10,000 rpm (10 min at room temperature), and separated on a NuPAGE® 4–12% Bis-Tris Gel using 1X NuPAGE® MOPS SDS Running Buffer. The proteins were transferred electrophoretically from the gel to a Bio-Rad Trans-Blot® Turbo™ 0.2 μm PVDF transfer membrane using a Bio-Rad Trans-Blot® Turbo™ transfer system. We blocked the membranes with an Odyssey blocking buffer for 1 h before incubating them overnight in the primary antibody solution, which contained anti-HIF-1α (diluted 1:1000), anti-CAIX (diluted to 1:200) anti-GAPDH (diluted 1:1000) in blocking buffer. Table S-3 lists the brand and specificity of primary and secondary antibodies used for immunoblotting. We washed the membranes in TBST (5 min × 3) before incubating them for 1 h in the secondary antibody solution, which contained IR Dye 680-conjugated donkey anti-rabbit IgG (diluted 1:10,000) in blocking buffer. We imaged the membranes using Odyssey CLX (LI-COR Biosciences) and analyzed them using Odyssey 2.1 Software. See Table S-3 for the description of the antibodies in detail.

2.10. Immunoassay for quantification of HGF levels in cells

We assayed the HGF levels of three isogenic lines of A549 cells using a Quantikine® ELISA from R&D Systems which utilized a sandwich immunoassay method, and followed the protocol recommended by the manufacturer. Prior to analysis, we seeded 2000 A549, A549-HGF, or A549-HGF-M cells into black-walled 96-well plates with clear bottom, and cultured the cells overnight. The absorbance of the solutions was measured using Spectramax at 450 nm; absorbance measurements were corrected by subtracting the absorbance at 540 nm to account for the optical imperfections of the well plate. The HGF concentration was calculated from the best-fit line obtained from a standard curve.

3. Results

3.1. Sensitivity to radiation decreases with increasing cellular densities

To determine if the density of cells in the single-layer cultures affected their response to radiation, we prepared single-layer cultures of A549 cells with cellular densities ranging from 2000 to 80,000 cells/zone and exposed them to ionizing radiation ranging from 0 to 16 Gy. We cultured the irradiated samples for an additional 6 days, to allow for multiple cellular divisions, before measuring the metabolic activities of the cells. We used Eq. (1) to determine changes in metabolic activity of cells undergoing radiation, where: $N_{L\ irrad,X\ Gy}$ is the luminescence intensity of the metabolically active cells in layer L, irradiated at X Gy; and $N_{L\ non-irrad}$ is the luminescence intensity of the metabolically active cells in the corresponding, non-irradiated layer.

$$\%\text{metabolic activity}_{\ \text{single-layer culture}} = \frac{N_{L\ irrad,X\ Gy}}{N_{non-irrad}} \times 100 \quad (1)$$

These results showed that the metabolic activity of the cells in the single-layer cultures, independent of cell seeding density, decreased with increasing dosages of irradiation. The magnitude of this decrease in metabolic activity is cell density dependent, however, and best illustrated when comparing samples containing 2000 and 80,000 cells/zone. In the 2000 cells/zone cultures, the metabolic activity decreased by values ranging from 78% to 85% (n = 3 scaffolds) when irradiated with 16 Gy. The metabolic activity 80,000 cells/zone cultures irradiated with the same dose decreased by values ranging from 26% to 35% (n = 3 scaffolds).

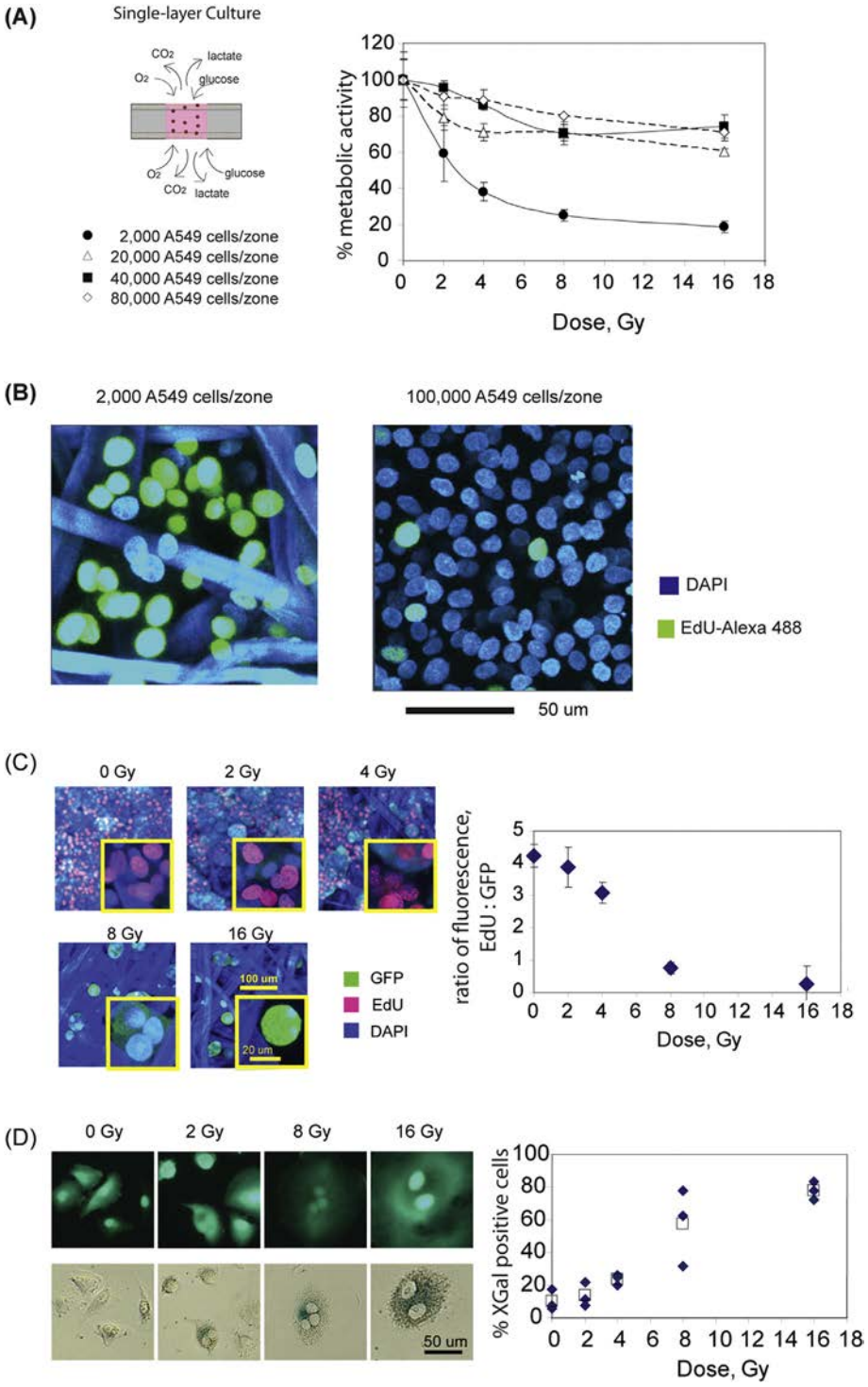

Fig. 2. Radiation response of single-layer cultures of A549-GFP cells. (A) Schematic of a zone of a single-layer culture (left) and graph showing the decrease in metabolic activity for single-layer cultures that were seeded at different densities post-irradiation (right). Each datum represents the ratio of irradiated and non-irradiated samples, error bars represent the standard deviation for n = 3 scaffolds. (B) Confocal fluorescence images of A549 cells stained with Click-iT® EdU Alexa Fluor® 488. Both images were taken at the same magnification. (C) Confocal fluorescence images of A549 cells stained with Click-iT® EdU Alexa Fluor® 594. The scale bar for all the images are found on the sample irradiated at 16 Gy—the top scale bar is for images at low magnification, while the bottom one is for images at high magnification. Graph showing the ratio of proliferating cells with surviving A549-GFP cells. The intensities of Alexa Fluor® 594 (proliferating A549-GFP cells) and GFP (surviving A549-GFP cells) were measured using a Typhoon scanner. Error bars represent the standard deviation for n = 10 zones. (D) Fluorescence (top) and bright field (bottom) images of A549-GFP cells labeled for senescence-associated β-galactosidase activity. All images were taken at the same magnification. Graph showing the percentage of senescent cells (stained with blue) with the total number of A549-GFP cells. Data points represent the % X-Gal for n = 3 wells. (For interpretation of the references to color in this figure legend, the reader is referred to the web version of this article.)

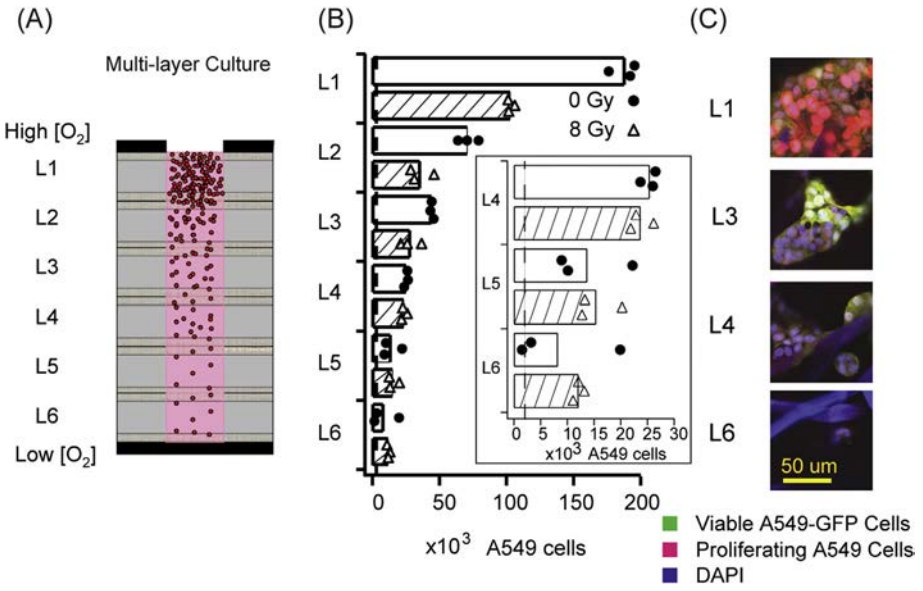

Fig. 3. Radiation response of cells in multi-layer cultures of A549 cells. (A) Schematic of a column of cells in a zone of the multi-layer culture stack. (B) Graph summarizing the number of metabolically-active cells in layers L1 to L6. Circular and triangular markers represent values obtained for non-irradiated and irradiated stacks, respectively; bars represent the average value of three stacks. (Inset) Enlarged graph for L4 to L6. The broken lines indicate the seeding density of cells in each layer. (C) Confocal fluorescence images of A549 cells in a non-irradiated, multi-layer culture showing decrease in the density of cells, and decrease in the incorporation of the proliferation stain, EdU (Click-iT® EdU Alexa Fluor® 594) from L1 to L6.

3.2. Increases in cellular density decrease cellular proliferation

Exposure to ionizing radiation can damage DNA [3,6,7,49,50], and the continued replication of unrepaired and defective DNA can result in cellular death [50]. We hypothesized that the reduced sensitivity of high densities of cells to radiation correlated with the rate in which these cells proliferate. To test this hypothesis, we cultured single-sheets containing either 2000 cells/zone or 100,000 cells/zone for seven days prior to labeling the proliferating cells with a Click-iT® EdU kit. Each sample was incubated in medium containing 5-ethynyl-2′-deoxyuridine (EdU), a thymidine analog that incorporates into the DNA of cells undergoing replication [51], prior to fixation and labeling with a Alexa Fluor® 594-conjugated azide [51]. Confocal fluorescence micrographs (Fig. 2B) revealed a higher fraction of proliferating cells, and the formation of larger spheres in single-layer cultures containing a lower seeding density. These results are consistent with previous studies showing that radiation-induced damage to cells is enhanced in cells undergoing proliferation.

3.3. Radiation-resistant cells in oxygen-rich environments are mostly non-proliferating and senescent

One possible explanation for the metabolically active cells that remain after irradiation with as much as 16 Gy is the surviving cells were senescent at the time of irradiation, or became senescent after irradiation [52]. To further characterize the metabolically active cells in well-oxygenated environments after irradiation, we cultured A549-GFP in single-layer composites overnight before irradiating the samples with doses ranging from 0 to 16 Gy. To enumerate proliferating cells, we used the EdU assay described above. To enumerate senescent cells, we incubated the samples in X-Gal (5-bromo-chloro-3-indolyl-β-D-galactopyranoside), a chromogenic substrate for β-galactosidase [53,54].

3.3.1. Most of the surviving cells do not proliferate

To approximate the ratio of the number of proliferating cells to the total number of cells that survived irradiation, we compared the fluorescence intensities of EdU-labeled cells and GFP. The graph in Fig. 2C indicates that cells surviving irradiation with at least 8 Gy were non-proliferative, or lost the ability to proliferate.

3.3.2. Most of the surviving cells are senescent

To determine if the surviving cells were senescent, we incubated the scaffolds in X-Gal and attempted to count the blue-colored cells with a bright-field microscope; this method was difficult because the cellulose fibers of the paper scatter light readily [41,47]. To more accurately count the senescent cells, we used Accumax to enzymatically degrade the Matrigel and recover the cells from the scaffold. We cultured the recovered cells for 48 h before staining with X-Gal.

Fluorescence and bright-field images (Fig. 2D) indicated the fraction of X-gal positive cells increased with increasing dosage of radiation: values ranging from 5% to 18% ($n = 3$ scaffolds) for non-irradiated cultures; and values ranging from 72% to 83% ($n = 3$ scaffolds) for cultures irradiated with 16 Gy. The micrographs also revealed the average size of the cells increased with increasing radiation dosage. Increased cell size is also a senescent phenotype (Fig. 2D) [53,54]. This data, which indicates cells surviving radiation dosages of at least 8 Gy are largely senescent, agrees with the proliferation data (Fig. 2C).

3.4. The availability of oxygen and nutrients influence radiation sensitivity in multi-layer cultures

To determine if cells cultured in different positions of the multi-layer stack have different sensitivities to ionizing radiation, we compared the metabolic activity of irradiated and non-irradiated stacks. We cultured the assembled stacks, depicted in Fig. 3A, for four days to ensure a gradient of oxygen formed in the cultures before irradiating half the samples with 8 Gy. Each stack was cultured for an additional seven days post-irradiation, and then analyzed with the CTG assay. Unless stated otherwise, radiation experiments for all multi-layer cultures were carried out as

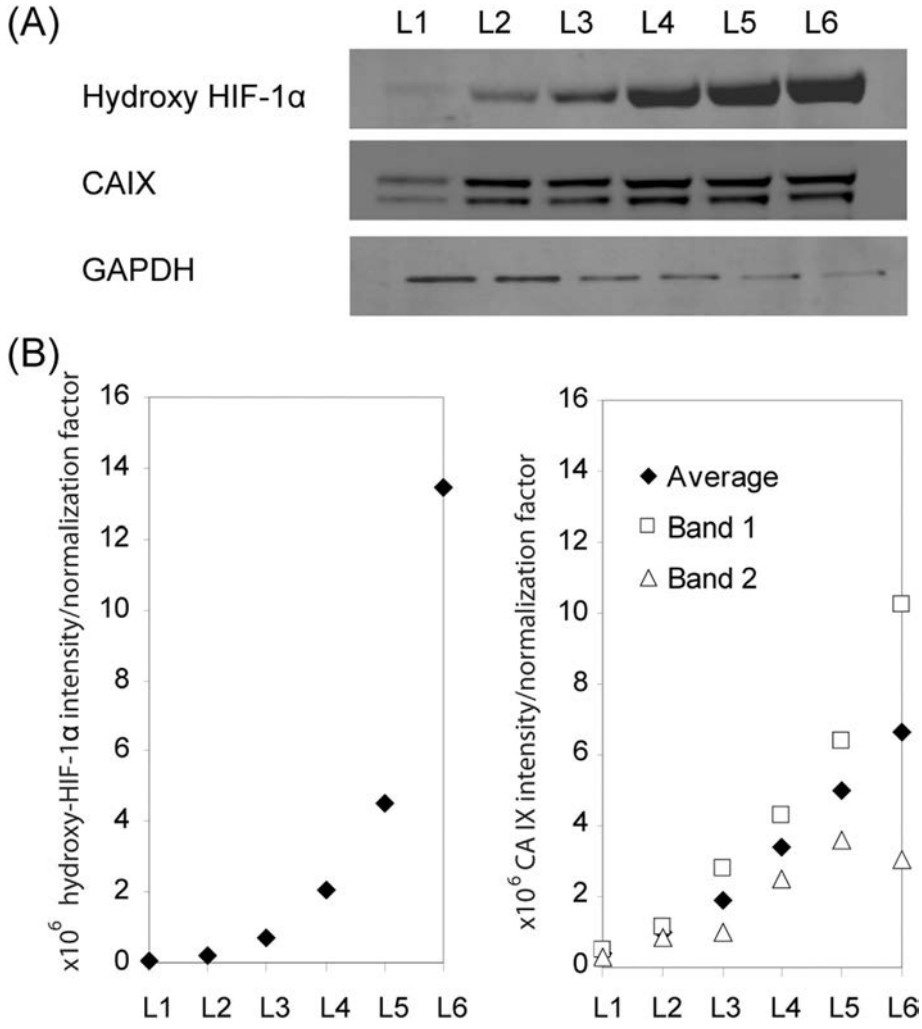

Fig. 4. Hydroxy-HIF-1α and CAIX expression of A549 cells in multi-layer cultures using Western blot. (A) Images of blots of A549 lysates carried out for hydroxy-HIF-1α, CAIX and GAPDH (loading control). CAIX is a dimeric protein, and results in two bands in the Western Blot. (B) Graph summarizing the ratio of hydroxyl-HIF-1α and CAIX intensities to a normalization factor, calculated from the ratio of the intensity of the band from GAPDH of each layer, to the intensity of the highest GAPDH among all the layers.

described above.

We compared the metabolic activity of each layer from the irradiated stack with its corresponding layer from the non-irradiated stack, and calculated the change in metabolic activity using Eq. (1). Reduction of metabolic activity was position-dependent and only occurred in layers close to the source of oxygen-rich culture medium (Fig. 3B). The metabolic activity of the cells in L1 and L2 decreased by values ranging from 35% to 59% (n = 6 scaffolds). The metabolic activity in L3 decreased by values ranging from 17% to 52% (n = 3 scaffolds). No statistically significant decrease was observed in L4 and L5. The responsiveness of the cells in L6 to irradiation is unclear because the mean is smaller than about twice the standard error for L6 of the non-irradiated stack (Table S-1a) [55].

We hypothesized the insensitivity of the cells at the bottom of the stack to radiation was due to decreased proliferation. We attributed this decreased proliferation to decreased oxygen tensions, resulting from the gradient formed from cells in the uppermost layers consuming the majority of the oxygen diffusing into the stack. To verify this hypothesis, we labeled the proliferating cells with EdU in the non-irradiated multi-layer culture of A549-GFP cells after 11 days of culture. Confocal images of the stained layers indicated a similar observation; the proliferation of cells is highest in L1 and is lowest in L6 (Fig. 3C).

Table 1
HGF levels released from overnight cultures of A549 and A549-derived lines.

Cell line	pg HGF/mL
A549	Not detected
A549-HGF	257 ± 36
A549-HGF-M	608 ± 71

3.5. Hypoxia markers expressed in cells increase with the distance of cells from the source of oxygenated medium

To verify the cells in different locations of the multi-layer cultures were experiencing different oxygen tensions, we measured the expression of two markers for hypoxia in each layer of the stack: (i) the hydroxylated form of hypoxia inducible factor 1-alpha (hydroxy-HIF-1α), which is the predominant form of this hypoxia-sensitive protein in well-oxygenated cells [56], and (ii) carbonic anhydrase 9 (CAIX), a protein whose expression is induced under

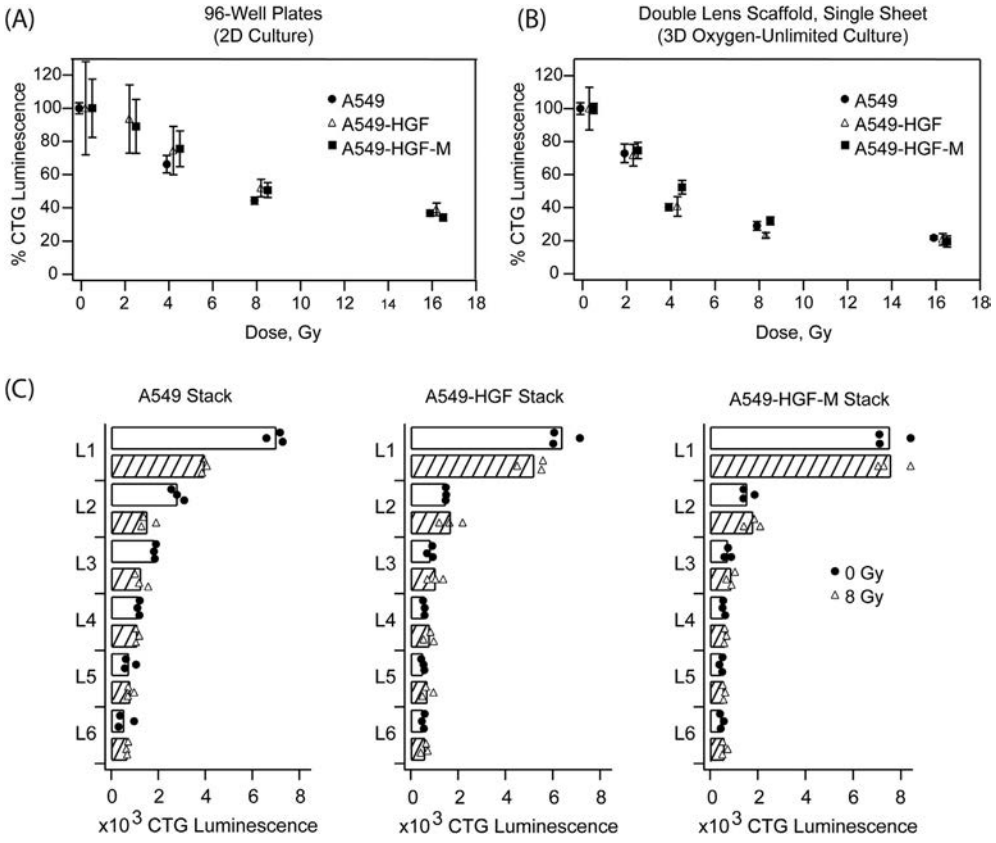

Fig. 5. Radiation response for lung carcinoma lines in different culture systems. Viability curves of A549, A549-HGF and A549-HGF-M in (A) 2D and (B) single-layer cultures. Error bars represent the standard deviation for n = 6 wells (96-well plates), and n = 3 sheets (PVC-lens paper composite). (C) Graphs summarizing the viability of A549, A549-HGF and A549-HGF-M in multi-layer cultures. Circular and triangular markers represent values obtained for non-irradiated and irradiated stacks, respectively; bars represent the average value of three stacks.

hypoxic conditions by HIF-1α [57–59]. The assembled stacks were cultured for 4 days prior to analyzing the expression levels of hydroxy-HIF-1α and CAIX in each layer by Western blot. To account for differences in total protein content in each lysate, we used glyceraldehyde 3-phosphate dehydrogenase (GAPDH) as a control, and normalized the signal of hydroxy-HIF-1α and CAIX to the total protein content. The Western blot showed an increasing amount of both the hydroxy-HIF-1α and CAIX bands from L1 to L6 when normalized by GAPDH (Fig. 4). These results support our assumptions that the monotonic gradients forming in the multi-layer cultures, oxygen specifically, affects the rate of cell proliferation and therefore their resistance to ionizing radiation.

3.6. *Multi-layer cultures can distinguish differences in the radiation response of cell lines that secrete different levels of hepatocyte growth factor*

We compared the radiation sensitivity of three isogenic cell lines of A549 cells: the parental line, cells engineered to constitutively overexpress hepatocyte growth factor (A549-HGF), and a sub-clone of A549-HGF cells that was collected from a metastatic tumor in the lung of a murine xenograft (A549-HGF-M). The parental A549 cells are known to be less metastatic *in vivo* than the HGF-expressing A549 variants [44]. Using a sandwich-based ELISA, we were unable to detect HGF in the A549 parental cell line while both A549-HGF and A549-HGF-M secreted significant levels of HGF (>250 pg HIF/mL, Table 1). HGF is known to increase cellular migration and proliferation [60,61] as well as decrease radiosensitivity. When cultured in a monolayer (Fig. 5A) or a single-layer culture (Fig. 5B), all three lines of A549 cells had similar decreases in metabolic activity with increasing dosages of radiation.

When cultured in the multi-layer stacks, cells that released the most HGF responded the least to irradiation (Fig. 5C): (i) A549-HGF-M cells, independent of their location in the stack, have no clear response to radiation (Tables S-2e,f); (ii) A549-HGF have an observable response in L1, a reduction ranging from 13% to 30% (n = 3 scaffolds, Tables S-2c,d); and (iii) wild-type A549 cells have a clear response in L1 through L3 (Tables S-2a,b). We hypothesized that the different HGF levels in the three cell lines contributed to the observed differences in radiosensitivity by affecting the proliferation or migration rate of the cells.

To better understand the effects of migration and proliferation during culture, we analyzed the irradiated multi-layer stacks of A549-HGF-M two, four, and six days post-irradiation. The metabolic activity of cells in the upper layers showed an observable decrease in viability between two and four days post-irradiation (Fig. 6A). The number of viable cells in each layer of the irradiated and non-irradiated stack match six days post-irradiation. These results suggest the cells can repopulate the top layers of the multi-layer cultures by proliferating rapidly, and/or migrating from the lower layers of the stack to the upper layers of the stack. Both of these events could account for the apparent unresponsiveness of A549-HGF-M cells to radiation seven days after irradiation.

To decouple the contribution of migration from proliferation in multi-layer cultures of A549-HGF-M cells, we separated the layers with sheets of polycarbonate filters with 0.20 μm diameter pores; these pores prevented cell migration during culture, but allowed diffusion of molecules (e.g., oxygen and glucose) throughout the

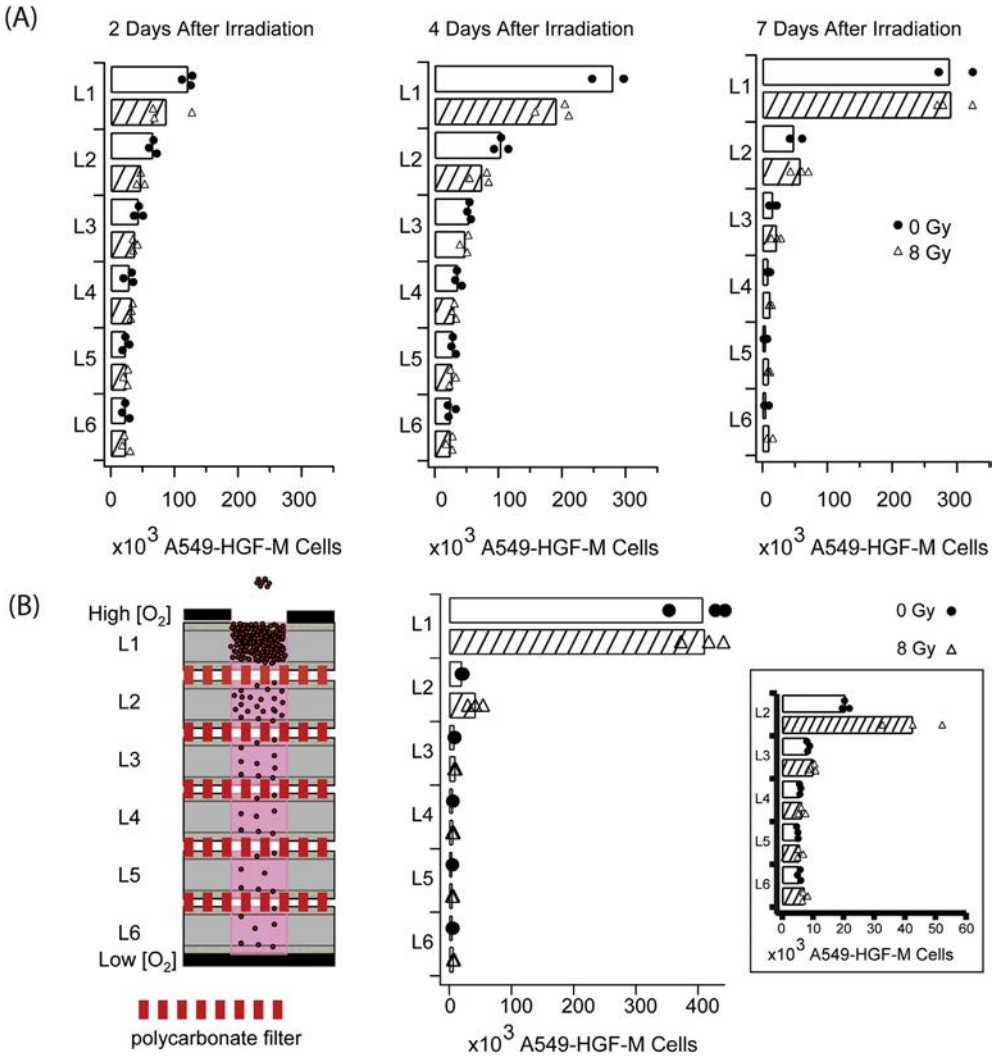

Fig. 6. Radiation response of A549-HGF-M in multi-layer culture. (A) Viability of multi-layer cultures of A549-HGF-M measured at different time points. (B) Viability of multi-layer cultures of A549-HGF-M with polycarbonate filters (pore diameter = 0.20 μm). (Inset) Enlarged graph for the viability of multi-layer cultures of A549-HGF-M from L2 to L6. Circular and triangular markers represent values obtained for non-irradiated and irradiated stacks, respectively; bars represent the average value of three stacks.

stack. The graph in Fig. 6B indicates that blocking migration does not enhance the sensitivity of cells to radiation, and thus suggests that the unresponsiveness we observed in long-term cultures of A549-HGF-M cells was due to proliferation, and not migration.

3.7. Manipulating the diffusion of oxygen before and after irradiation show that the presence of oxygen is critical after irradiation

The results from the multi-layer culture experiments show that the gradient of oxygen causes differences in cellular proliferation and radiosensitivity within the layers of the stack; these results however, do not indicate if oxygen is critical to cell survival during or after irradiation. We prepared a number of experiments to determine if there was a difference in radiosensitivity for cells that were assembled into a multi-layer stack prior to irradiation (Fig. 7A) or assembled into a multi-layer stack after the single-layer stacks were irradiated (Fig. 7B). We also altered the time of culture before destacking the multilayer culture to determine if the response to radiation changed. Our results have consistently shown cellular radiosensitivity decreased from L1 to L6 when cultured as a stack after irradiation; this trend can be observed even in cells cultured and irradiated as single layers and then were stacked after irradiation (Fig. 7A). On the other hand, radiosensitivity was observed in all layers upon de-stacking; radiosensitive cells were observed even in regions likely deprived of oxygen (i.e., L4 and L6) prior to irradiation (Fig. 7B). The oxygen dependence observed within the irradiated stack, and the increase in radiosensitivity of cells in all the layers shortly after de-stacking suggests that oxygenation of A549 cells after irradiation is a crucial determinant of the response of these cells to radiation.

4. Discussion

The paper-based cell culture system we describe in this work offers many advantages over the monolayer and spheroid cultures currently used in radiation studies because: (i) millimeter-thick cultures—the scale of thickness relevant to solid tumors—can be generated by simply stacking the single-layer composite sheets; (ii) the diffusion-dominated environment of the culture allows cells experiencing different concentrations of nutrients, waste products, and drugs to be studied simultaneously; (iii) each sheet in the stack can potentially contain different types of cells and/or gels for co-culture and/or extracellular matrix (ECM) studies; (iv) the multi-

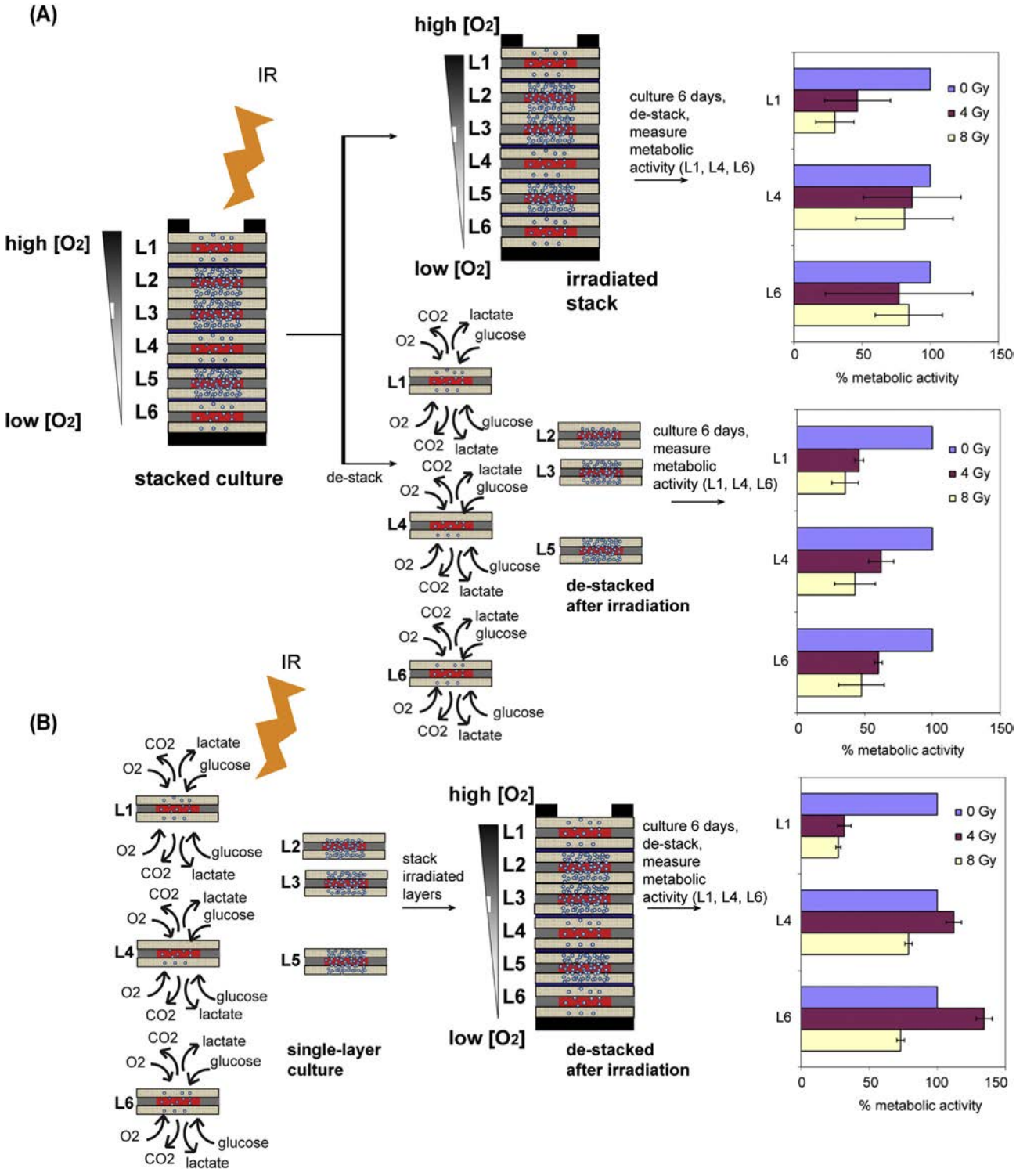

Fig. 7. Manipulation of oxygen in irradiation experiments. Schematic and accompanying graph of cellular viability for cells in multi-layer cultures that were cultured either as (A) stacks or as (B) single-layers prior to irradiation. To generate a steep gradient, layers containing high density of cells (i.e., L2, L3, L5), separated with polycarbonate filters (pore diameter = 0.20 μm), were placed between the layers to be analyzed (i.e., L1, L4, L6). Error bars represent the standard deviation for n = 3 stacks.

layer stack can be sectioned easily by peeling the layers apart and does not require histology equipment; (v) the separated sheets can be analyzed optically or through the use of enzymatic assays; and (vi) the sheets can be patterned using the fabrication method described above to create multi-zone patterns that can be adapted for high-throughput assays [42,46,47].

Using this *in vitro* system, we were able to demonstrate, that decreasing levels of oxygen can reduce the proliferation of non-small cell lung cancer cells, and consequently, reduce their metabolic sensitivity to ionizing radiation. The concomitant reduction of

cellular proliferation and radiosensitivity with low oxygen tensions has been observed consistently not only in tumors [62], but also *in vitro* cultures [63,64]. We confirmed cells that are placed at increasing distances from the source of oxygen and media in the multi-layer culture show increased expression of HIF-1α and CAIX, indicating these cells are experiencing decreasing oxygen tensions (e.g., hypoxia); a trend that is also observed in tumors *in vivo*. HIF-1α has a half-life of less than 1 min [65] in re-oxygenated tumors, and is predominately in its hydroxylated form [66–69]. We expect that most of the HIF-1α proteins were hydroxylated at the time of analysis due to the time required to destack and stain the cells in the multi-layer cultures. It is therefore not surprising that the expression of hydroxy-HIF-1α is lowest in L1 and highest in L6. These results confirm that cells far from the source of oxygen are indeed hypoxic, and their insensitivity to radiation is in agreement with the widely held view that gradients of oxygen present in a tumor directly affect their sensitivity to radiation. These results are consistent with the response observed in solid tumors *in vivo*: cells in close proximity to blood vessels (i.e., < 200 μm) respond to radiation, and cells residing beyond this distance, which is believed to be a hypoxic environment, are less sensitive to irradiation [70–73]. Our results also emphasize that the presence of these oxygen gradients are as, if not more, influential post-treatment than during treatment. Our results further show the influence of oxygen on metabolic activity, and consequently proliferation-driven DNA damage response to radiation.

The multi-layer system also enabled us to distinguish the metabolic response to radiation of A549 and two of its HGF-secreting variants; our findings are consistent with those *in vivo*, and are more predictive than 2D, single-layer cultures. These results, therefore, demonstrate that multi-layer cultures can serve as an *in vitro* system for studying biological processes such as radiation response, while taking into account factors that are native to tumor biology such as limitations of mass transport and migration of cells.

Although the observation in which the highly-proliferative variants of A549 cells have higher radioresistance than the A549 parental line seemed to contradict our earlier findings that oxygen-driven proliferation increased radiosensitivity, the increased expression of HGF does not only increase proliferation, but is also associated resistance to chemotherapy and radiotherapy, and cancer stemness [74–76]. The radioresistance of the A549-producing variants therefore involve a mechanism more complicated than oxygen-driven proliferation.

We also demonstrate that this system is compatible with assays for measuring cellular metabolism (Cell-Titer-Glo assay), proliferation (Click-iT Edu assay) and senescence (X-Gal staining). These assays characterize different aspects of cellular response to radiation, and are amenable to high-throughput screening assays routinely performed in the pharmaceutical industry. We note that survival curves are of particular interest to radiobiologists, and although not performed provide complementary information to the assays described in this work.

We also highlight the utility of assembling and disassembling the stack to manipulate oxygen levels in the cultures. Alterations in the sequence of stacking and de-stacking the multi-layer cultures enabled us to supply or deprive cells of oxygen at different points of an irradiation experiment. Our results show that oxygen levels after irradiation are likely the primary determinant of cell survival. Studies such as this are challenging, if not impractical in traditional 3D culture systems.

5. Conclusion

This work describes a paper-based 3D culture system that can distinguish the metabolic sensitivity of cells to ionizing radiation, within gradients of small molecules of oxygen, nutrients, and autocrine factors, using a single setup. These gradients are also present in tumors *in vivo* and in spheroid cultures, but the advantage of the CiGiP system is it allows for precise isolation of cells within these gradients for quantification of metabolic activity, and also allows for direct manipulation of the cell density to alter the steepness of these gradients. Using this system, we were able to decouple effects of proliferation and migration by leveraging the unique stacking features of this system.

The current disadvantage of the system is it must be disassembled prior to analysis, preventing multiple measurements to be taken over time as the gradients that formed in the culture are destroyed. Incorporating sensors into the layers, for example, printing electrodes to measure oxygen concentration or pH, offer the potential of monitoring cellular activities in the multi-layer cultures while maintaining the fidelity of the molecular gradients formed in the stack. Integrating a sensing system to the 3D culture system that could quantify oxygen concentration within the stack will enable direct assessment of the influence of oxygen levels on cellular phenotype.

We believe this approach can be further used to evaluate the response of different tumors under different oxygen tensions to radiation, while taking into account differences in the rates of proliferation and migration of the cells within the population. The dynamics would be particularly interesting when studying the heterogeneous populations of cells found in the tumor environment (e.g., stromal cells) [43]. The study of the interaction between tumor cells with stromal cells, co-cultured in this multi-layer culture system, is among our group's current work. We believe this system also has the potential to be used as an *in vitro* assay for evaluating drugs that target hypoxic cells, or to evaluate the resistance of cells to radiation over long periods (i.e., weeks) post-treatment.

The simplicity of the CiGiP system, with minimal required equipment, will enable users from a broad-range of disciplines to adopt this technology in their own radiation studies.

Acknowledgements

This work was funded in part by Vertex Pharmaceuticals Incorporated. We thank the Wyss Institute for Biologically Inspired Engineering for providing funds to BM.

Appendix A. Supplementary data

Supplementary data related to this article can be found at http://dx.doi.org/10.1016/j.biomaterials.2016.03.002.

References

[1] American Cancer Society, Cancer Facts and Figures 2014, American Cancer Society, Atlanta, 2014.
[2] A. Jemal, R. Siegel, E. Ward, T. Murray, J. Xu, C. Smigal, et al., Cancer statistics, CA Cancer J. Clin. 2006 (56) (2006) 106–130.
[3] S.P. Jackson, J. Bartek, The DNA-damage response in human biology and disease, Nature 461 (2009) 1071–1078.
[4] A.C. Begg, F.A. Stewart, C. Vens, Strategies to improve radiotherapy with targeted drugs, Nat. Rev. Cancer 11 (2011) 239–253.
[5] G.C. Barnett, C.M.L. West, A.M. Dunning, R.M. Elliott, C.E. Coles, P.D.P. Pharoah, et al., Normal tissue reactions to radiotherapy: towards tailoring treatment dose by genotype, Nat. Rev. Cancer 9 (2009) 134–142.
[6] J.P. Pouget, T. Douki, M.J. Richard, J. Cadet, DNA damage induced in cells by gamma and UVA radiation as measured by HPLC/GC-MS and HPLC-EC and Comet assay, Chem. Res. Toxicol. 13 (2000) 541–549.
[7] J.F. Ward, DNA damage produced by ionizing radiation in mammalian cells: identities, mechanisms of formation, and reparability, Prog. Nucleic Acid Res. Mol. Biol. 35 (1988) 95–125.
[8] J.E. Biaglow, The effects of ionizing radiation on mammalian cells, J. Chem.

Educ. 58 (1981) 144.
[9] H. Houtgraaf Jaco, J. Versmissen, J. van der Giessen Wim, A concise review of DNA damage checkpoints and repair in mammalian cells, Cardiovasc. Revasc. Med. 7 (2006) 165–172.
[10] P. Schuller, S. Puttmann, R. Mucke, V. Senner, U. Schafer, K. Kisters, et al., From the radiolysis of water to the role of trace elements in radiobiology and clinical radiation therapy: following a logical chain, Trace Elem. Electrolytes 18 (2001) 186–192.
[11] J. Anastassopoulou, Free radicals in biology and medicine, Asian Chem. Lett. 2 (1998) 1–6.
[12] P. Jeggo, M.F. Lavin, Cellular radiosensitivity: how much better do we understand it? Int. J. Radiat. Biol. 85 (2009) 1061–1081.
[13] M.R. Lieber, Pathological and physiological double-strand breaks: roles in cancer, aging, and the immune system, Am. J. Pathol. 153 (1998) 1323–1332.
[14] R.J. Reiter, J.M. Guerrero, J.J. Garcia, D. Acuna-Castroviejo, Reactive oxygen intermediates, molecular damage, and aging; relation to melatonin, Ann. N. Y. Acad. Sci. 854 (1998) 410–424.
[15] K. Valerie, A. Yacoub, M.P. Hagan, D.T. Curiel, P.B. Fisher, S. Grant, et al., Radiation-induced cell signaling: inside-out and outside-in, Mol. Cancer Ther. 6 (2007) 789–801.
[16] A. Sancar, L.A. Lindsey-Boltz, K. Unsal-Kacmaz, S. Linn, Molecular mechanisms of mammalian DNA repair and the DNA damage checkpoints, Annu. Rev. Biochem. 73 (2004) 39–85.
[17] H. Lans, J.A. Marteijn, W. Vermeulen, ATP-dependent chromatin remodeling in the DNA-damage response, Epigenet. Chromatin. 5 (2012) 4.
[18] X. Huang, T. Tran, L. Zhang, R. Hatcher, P. Zhang, DNA damage-induced mitotic catastrophe is mediated by the Chk1-dependent mitotic exit DNA damage checkpoint, Proc. Natl. Acad. Sci. U. S. A. 102 (2005) 1065–1070.
[19] F. Bunz, A. Dutriaux, C. Lengauer, T. Waldman, S. Zhou, J.P. Brown, et al., Requirement for p53 and p21 to sustain G2 arrest after DNA damage, Science 282 (1998) 1497–1501.
[20] H. Vakifahmetoglu, M. Olsson, B. Zhivotovsky, Death through a tragedy: mitotic catastrophe, Cell Death Differ. 15 (2008) 1153–1162.
[21] S. Rockwell, I.T. Dobrucki, E.Y. Kim, S.T. Marrison, V.T. Vu, Hypoxia and radiation therapy: past history, ongoing research, and future promise, Curr. Mol. Med. 9 (2009) 442–458.
[22] R.H. Thomlinson, L.H. Gray, The histological structure of some human lung cancers and the possible implications for radiotherapy, Br. J. Cancer 9 (1955) 539–549.
[23] K. Groebe, P. Vaupel, Evaluation of oxygen diffusion distances in human breast cancer xenografts using tumor-specific in vivo data: role of various mechanisms in the development of tumor hypoxia, Int. J. Radiat. Oncol. Biol. Phys. 15 (1988) 691–697.
[24] P.T. Schumacker, R.W. Samsel, Analysis of oxygen delivery and uptake relationships in the Krogh tissue model, J. Appl. Physiol. 67 (1989) 1234–1244.
[25] D. Hanahan, R.A. Weinberg, The hallmarks of cancer, Cell 100 (2000) 57–70.
[26] J.M. Brown, W.R. Wilson, Exploiting tumour hypoxia in cancer treatment, Nat. Rev. Cancer 4 (2004) 437–447.
[27] J.M. Brown, A.J. Giaccia, The unique physiology of solid tumors: opportunities (and problems) for cancer therapy, Cancer Res. 58 (1998) 1408–1416.
[28] L.B. Harrison, M. Chadha, R.J. Hill, K. Hu, D. Shasha, Impact of tumor hypoxia and anemia on radiation therapy outcomes, Oncologist 7 (2002) 492–508.
[29] H. Harada, How can we overcome tumor hypoxia in radiation therapy? J. Radiat. Res. (Tokyo) 52 (2011) 545–556.
[30] M. Nordsmark, M. Overgaard, J. Overgaard, Pretreatment oxygenation predicts radiation response in advanced squamous cell carcinoma of the head and neck, Radiother. Oncol. 41 (1996) 31–39.
[31] L.H. Gray, A.D. Conger, M. Ebert, S. Hornsey, O.C. Scott, The concentration of oxygen dissolved in tissues at the time of irradiation as a factor in radiotherapy, Br. J. Radiol. 26 (1953) 638–648.
[32] D.M. Aebersold, P. Burri, K.T. Beer, J. Laissue, V. Djonov, R.H. Greiner, et al., Expression of hypoxia-inducible factor-1alpha: a novel predictive and prognostic parameter in the radiotherapy of oropharyngeal cancer, Cancer Res. 61 (2001) 2911–2916.
[33] P. Vaupel, A. Mayer, Hypoxia in cancer: significance and impact on clinical outcome, Cancer Metastasis Rev. 26 (2007) 225–239.
[34] L.G. Griffith, M.A. Swartz, Capturing complex 3D tissue physiology in vitro, Nat. Rev. Mol. Cell Biol. 7 (2006) 211–224.
[35] J.B. Kim, Three-dimensional tissue culture models in cancer biology, Semin. Cancer Biol. 15 (2005) 365–377.
[36] Y.C. Tung, A.Y. Hsiao, S.G. Allen, Y.S. Torisawa, M. Ho, S. Takayama, High-throughput 3D spheroid culture and drug testing using a 384 hanging drop array, Analyst 136 (2011) 473–478.
[37] G. Mehta, Y. Hsiao Amy, M. Ingram, D. Luker Gary, S. Takayama, Opportunities and challenges for use of tumor spheroids as models to test drug delivery and efficacy, J. Control. Release 164 (2012) 192–204.
[38] P.L. Olive, R.E. Durand, Drug and radiation resistance in spheroids: cell contact and kinetics, Cancer Metastasis Rev. 13 (1994) 121–138.
[39] E.M. Weaver, A.B. Hummon, Imaging mass spectrometry: from tissue sections to cell cultures, Adv. Drug Deliv. Rev. 65 (2013) 1039–1055.
[40] A.I. Minchinton, I.F. Tannock, Drug penetration in solid tumours, Nat. Rev. Cancer 6 (2006) 583–592.
[41] R. Derda, A. Laromaine, A. Mammoto, S.K.Y. Tang, T. Mammoto, D.E. Ingber, et al., Paper-supported 3D cell culture for tissue-based bioassays, Proc. Natl. Acad. Sci. U. S. A. 106 (2009) 18457–18462. S/1-S/9.
[42] R. Derda, S.K.Y. Tang, A. Laromaine, B. Mosadegh, E. Hong, M. Mwangi, et al., Multizone paper platform for 3D cell cultures, PLoS One 6 (2011) e18940.
[43] B. Mosadegh, B.E. Dabiri, M.R. Lockett, R. Derda, P. Campbell, K.K. Parker, et al., Three-dimensional paper-based model for cardiac ischemia, Adv. Healthc. Mater. 3 (2014) 1036–1043.
[44] B. Mosadegh, M.R. Lockett, K.T. Minn, K.A. Simon, K. Gilbert, S. Hillier, et al., A paper-based invasion assay: assessing chemotaxis of cancer cells in gradients of oxygen, Biomaterials 52 (2015) 262–271.
[45] F. Deiss, A. Mazzeo, E. Hong, D.E. Ingber, R. Derda, G.M. Whitesides, Platform for high-throughput testing of the effect of soluble compounds on 3D cell cultures, Anal. Chem. (Washington, DC, U S) 85 (2013) 8085–8094.
[46] F. Deiss, W.L. Matochko, N. Govindasamy, E.Y. Lin, R. Derda, Flow-through synthesis on teflon-patterned paper to produce peptide arrays for cell-based assays, Angew. Chem. Int. Ed. 53 (2014) 6374–6377.
[47] K.A. Simon, K.M. Park, B. Mosadegh, A.B. Subramaniam, A.D. Mazzeo, P.M. Ngo, et al., Polymer-based mesh as supports for multi-layered 3D cell culture and assays, Biomaterials 35 (2014) 259–268.
[48] S.P.M. Crouch, R. Kozlowski, K.J. Slater, J. Fletcher, The use of ATP bioluminescence as a measure of cell proliferation and cytotoxicity, J. Immunol. Methods 160 (1993) 81–88.
[49] J.E. Biaglow, The effects of ionizing radiation on mammalian cells, J. Chem. Educ. 58 (1981) 144–156.
[50] E. Cohen-Jonathan, E.J. Bernhard, W.G. McKenna, How does radiation kill cells? Curr. Opin. Chem. Biol. 3 (1999) 77–83.
[51] A. Salic, T.J. Mitchison, A chemical method for fast and sensitive detection of DNA synthesis in vivo, Proc. Natl. Acad. Sci. U. S. A. 105 (2008) 2415–2420.
[52] J. Campisi, F. d'Adda di Fagagna, Cellular senescence: when bad things happen to good cells, Nat. Rev. Mol. Cell Biol. 8 (2007) 729–740.
[53] G.P. Dimri, X. Lee, G. Basile, M. Acosta, G. Scott, C. Roskelley, et al., A biomarker that identifies senescent human cells in culture and in aging skin in vivo, Proc. Natl. Acad. Sci. U. S. A. 92 (1995) 9363–9367.
[54] J. Chen, M.S. Goligorsky, Premature senescence of endothelial cells: Methusaleh's dilemma, Am. J. Physiol. Heart Circ. Physiol. 290 (2006) H1729–H1739.
[55] D.G. Altman, J.M. Bland, Standard deviations and standard errors, BMJ Br. Med. J. 331 (2005) 903.
[56] C.E. Snell, H. Turley, A. McIntyre, D. Li, M. Masiero, C.J. Schofield, et al., Proline-hydroxylated hypoxia-inducible factor 1α (HIF-1α) upregulation in human tumours, PLoS One 9 (2014) e88955.
[57] P. Swietach, A. Hulikova, R.D. Vaughan-Jones, A.L. Harris, New insights into the physiological role of carbonic anhydrase IX in tumour pH regulation, Oncogene 29 (2010) 6509–6521.
[58] S.K. Parks, J. Chiche, J. Pouyssegur, pH control mechanisms of tumor survival and growth, J. Cell. Physiol. 226 (2011) 299–308.
[59] M.C. Brahimi-Horn, J. Chiche, J. Pouysségur, Hypoxia and cancer, J. Mol. Med. 85 (2007) 1301–1307.
[60] A.A. Sadiq, R. Salgia, MET as a possible target for non-small-cell lung cancer, J. Clin. Oncol. 31 (2013) 1089–1096.
[61] G. Maulik, A. Shrikhande, T. Kijima, P.C. Ma, P.T. Morrison, R. Salgia, Role of the hepatocyte growth factor receptor, c-Met, in oncogenesis and potential for therapeutic inhibition, Cytokine Growth Factor Rev. 13 (2002) 41–59.
[62] P. Carmeliet, Y. Dor, J.-M. Herbert, D. Fukumura, K. Brusselmans, M. Dewerchin, et al., Role of HIF-1[alpha] in hypoxia-mediated apoptosis, cell proliferation and tumour angiogenesis, Nature 394 (1998) 485–490.
[63] G. Xue, Z. Ren, P.W. Grabham, Y. Chen, J. Zhu, Y. Du, et al., Reprogramming mediated radio-resistance of 3D-grown cancer cells, J. Radiat. Res. (Tokyo) 56 (2015) 656–662.
[64] I. Eke, N. Cordes, Radiobiology goes 3D: how ECM and cell morphology impact on cell survival after irradiation, Radiother. Oncol. 99 (2011) 271–278.
[65] A.Y. Yu, M.G. Frid, L.A. Shimoda, C.M. Wiener, K. Stenmark, G.L. Semenza, Temporal, spatial, and oxygen-regulated expression of hypoxia-inducible factor-1 in the lung, Am. J. Physiol. 275 (1998) L818–L826.
[66] G.L. Semenza, HIF-1: upstream and downstream of cancer metabolism, Curr. Opin. Genet. Dev. 20 (2010) 51.
[67] K. Hirota, G.L. Semenza, Regulation of hypoxia-inducible factor 1 by prolyl and asparaginyl hydroxylases, Biochem. Biophys. Res. Commun. 338 (2005) 610–616.
[68] P. Jaakkola, D.R. Mole, Y.-M. Tian, M.I. Wilson, J. Gielbert, S.J. Gaskell, et al., Targeting of HIF-α to the von Hippel-Lindau ubiquitylation complex by O2-regulated prolyl hydroxylation, Science 292 (2001) 468–472.
[69] P.H. Maxwell, M.S. Wiesener, G.W. Chang, S.C. Clifford, E.C. Vaux, M.E. Cockman, et al., The tumour suppressor protein VHL targets hypoxia-inducible factors for oxygen-dependent proteolysis, Nature 399 (1999) 271–275.
[70] P. Vaupel, Tumor microenvironmental physiology and its implications for radiation oncology, Semin. Radiat. Oncol. 14 (2004) 198–206.
[71] J. Varlotto, M.A. Stevenson, Anemia, tumor hypoxemia, and the cancer patient, Int. J. Radiat. Oncol. Biol. Phys. 63 (2005) 25–36.
[72] M. Bache, M. Kappler, H.M. Said, A. Staab, D. Vordermark, Detection and specific targeting of hypoxic regions within solid tumors: current preclinical and clinical strategies, Curr. Med. Chem. 15 (2008) 322–338.
[73] J.L. Tatum, G.J. Kelloff, R.J. Gillies, J.M. Arbeit, J.M. Brown, K.S. Chao, et al., Hypoxia: importance in tumor biology, noninvasive measurement by imaging, and value of its measurement in the management of cancer therapy, Int. J. Radiat. Biol. 82 (2006) 699–757.
[74] V. Bhardwaj, T. Cascone, M.A. Cortez, A. Amini, J. Evans, R.U. Komaki, et al.,

Modulation of c-Met signaling and cellular sensitivity to radiation, Cancer 119 (2013) 1768–1775.
[75] K.P.S. Raghav, A.M. Gonzalez-Angulo, G.R. Blumenschein, Role of HGF/MET axis in resistance of lung cancer to contemporary management, Transl. Lung Cancer Res. 1 (2012) 179–193.
[76] C. Boccaccio, P.M. Comoglio, The MET oncogene in glioblastoma stem cells: implications as a diagnostic marker and a therapeutic target, Cancer Res. 73 (2013) 3193–3199.